Analysis of the Composite Response of Shear Wave Resonators to the Attachment of Mammalian Cells

Joachim Wegener, Jochen Seebach, Andreas Janshoff, and Hans-Joachim Galla

Institut für Biochemie, Westfälische Wilhelms-Universität Münster, 48149 Münster, Germany

ABSTRACT   The suitability of the quartz crystal microbalance (QCM) technique for monitoring the attachment and spreading of mammalian cells has recently been established. Different cell species were shown to generate an individual response of the QCM when they make contact with the resonator surface. Little is known, however, about the underlying mechanisms that determine the QCM signal for a particular cell type. Here we describe our results for different experimental approaches designed to probe the particular contributions of various subcellular compartments to the overall QCM signal. Using AC impedance analysis in a frequency range that closely embraces the resonators' fundamental frequency, we have explored the signal contribution of the extracellular matrix, the actin cytoskeleton, the medium that overlays the cell layer, as well as the liquid compartment that is known to exist between the basal plasma membrane and the culture substrate. Results indicate that the QCM technique is only sensitive to those parts of the cellular body that are involved in cell substrate adhesion and are therefore close to the resonator surface. Because of its noninvasive nature, sensitivity, and time resolution, the QCM is a powerful means of quantitatively studying various aspects of cell-substrate interactions.

INTRODUCTION

Cultured animal cells have gained increasing importance as model systems in many branches of fundamental and applied biomedical research. The scientific impacts of these model systems might be improved in manifold ways if more potent methods were to be made available that are capable of monitoring morphological aspects of cultured cells under defined experimental conditions in a quantitative and non-invasive way. Lately, the quartz crystal microbalance (QCM) technique has attracted considerable interest as a novel means of performing such measurements. The QCM is based on a thin (AT-cut) quartz disk sandwiched between two metal electrodes. As the quartz crystal is piezoelectric in nature, an oscillating potential difference between the surface electrodes leads to corresponding shear displacements of the quartz disk. This mechanical oscillation is very sensitive to any changes that occur at the crystal surfaces, so that throughout the last few decades the QCM has been established as a reliable and sensitive technique for monitoring adsorption processes at solid/gas or solid/liquid interfaces (Sauerbrey, 1959; Buttry and Ward, 1992; Martin et al., 1991). Because of the simplicity of the experimental requirements and the outstanding sensitivity, most work in this field has utilized the resonance frequency of the shear oscillation as the measured quantity. The list of applications comprises thickness monitoring during the deposition of thin metal films from vapor phase (Sauerbrey, 1959), growth rate control during electrodeposition of polymer

films from solution (Bandey et al., 1997), and even the detection of molecular recognition events when the quartz surface is made specifically functional with receptors and a ligand is offered from solution (Janshoff et al., 1996a). It is important to recognize, however, that the shear oscillation is not only sensitive to mass deposition on the quartz surface but is also affected by changes in viscoelasticity of the material in contact with the resonator.

When quartz resonators are used as culture substrates for anchorage-dependent animal cells, the QCM technique is capable of probing the interactions of the cells with the resonator surface. Previously we (Wegener et al., 1998) and others (Gryte et al., 1993; Redepenning et al., 1993) have demonstrated that it is possible to follow the attachment and spreading of initially suspended mammalian cells on the resonator surface in real time by resonance frequency recordings. Such measurements provide the kinetics of cell attachment with a time resolution of less than 1 s. For example, we were able to measure quantitatively the distinct change in adhesion behavior of MDCK-II cells for two different temperatures and the impact of anti-adhesive peptides like Arg-Gly-Asp (RGD) on attachment kinetics. When comparing different cell lines under otherwise identical experimental conditions, we found that these different cell lines caused individual shifts of the resonance frequency (Wegener et al., 1998). This indicates that cell-type-specific mechanical properties may be inferred from QCM measurements. However, to interpret QCM data in terms of mechanical properties of the attached cells, it is necessary to describe the experimental situation by an appropriate physical model that contains these cellular properties as adjustable parameters. But the development of a reasonable model requires first of all a more detailed understanding of the signal sources. For instance, it is crucial to know which parts of the cellular body actually contribute to the measured QCM response. Once the underlying principles are

---

fully disclosed, there may be new areas of application, even in whole-cell biosensor devices that have not been considered so far.

Thus we report here a variety of experimental approaches designed to provide greater insight into the mechanisms that govern the response of shear wave resonators to the adhesion of mammalian cells. Because interpretation of the resonance frequency as the only measured quantity can be ambiguous when the resonator is loaded with a complex material like an attached cell layer, we performed an AC impedance analysis of the loaded crystal in the vicinity of its resonance frequency instead. Impedance measurements over a range of frequencies near resonance provide a more comprehensive and detailed description of the shear oscillation (Yang and Thompson, 1993). By this means we have quantified the QCM response for five different cell species of epithelial, endothelial, or fibroblastic nature. We have critically examined the role of extracellular matrix proteins beneath the cells and the contribution of the medium that overlays the cell layer. We have evaluated the impact of the actin cytoskeleton, and we furthermore report the changes in the QCM parameters that are associated with the application of hyperosmotic medium and the corresponding cell shrinkage. In particular, the experiments employing hyperosmotic conditions provide valuable hints about the contribution of the aqueous compartment that is known to exist between the basal cell membrane and any growth substrate.

MATERIALS AND METHODS

Quartz crystal microbalance setup and measurement

The QCM setup sketched in Fig. 1 *A* has been described in more detail elsewhere (Janshoff et al., 1996b). Briefly, we used plano-plano AT-cut quartz resonators ($\phi = 14$ mm) with a fundamental resonance frequency of 5 MHz, with circular gold electrodes ($\phi = 6$ mm) on both sides (KVG, Niederbischofsheim, Germany). The measuring chambers were made by mounting glass cylinders ($\phi = 10$ mm) on the quartz disks with a silicone adhesive (Rhône-Poulenc, Leverkusen, Germany). As we chose glass cylinders with threaded tops, the complete dishes could be closed with screw caps and handled like ordinary cell culture vessels. The quartz dish was clamped into the crystal holder as sketched in Fig. 1 *A* and connected to the continuous-wave impedance analyzer (SI-1260; Solartron Instruments, Farnborough, UK) by shielded cables.

Impedance analysis was performed at 250 equally spaced data points in a frequency range from 4.97 to 5.04 MHz, using a sinusoidal excitation voltage of 300-mV amplitude (peak-to-peak). Fig. 2 shows impedance data in a Bode presentation as typically recorded for quartz resonators covered with a confluent monolayer of MDCK-II cells (*empty circles*) or with culture medium only (*filled circles*). For data analysis we used the lumped-element Butterworth-Van-Dyke (BVD) equivalent circuit (Fig. 1 *B*), which consists of a capacitor C_0 paralleled by a series combination of an inductance L, a resistor R, and a capacitor C. The combination of L, R, and C is often referred to as the motional branch of the equivalent circuit, as only these impedance elements are associated with the shear motion of the quartz and are used for its description (Yang and Thompson, 1993). The parallel capacitance C_0 arises primarily from the presence of the dielectric
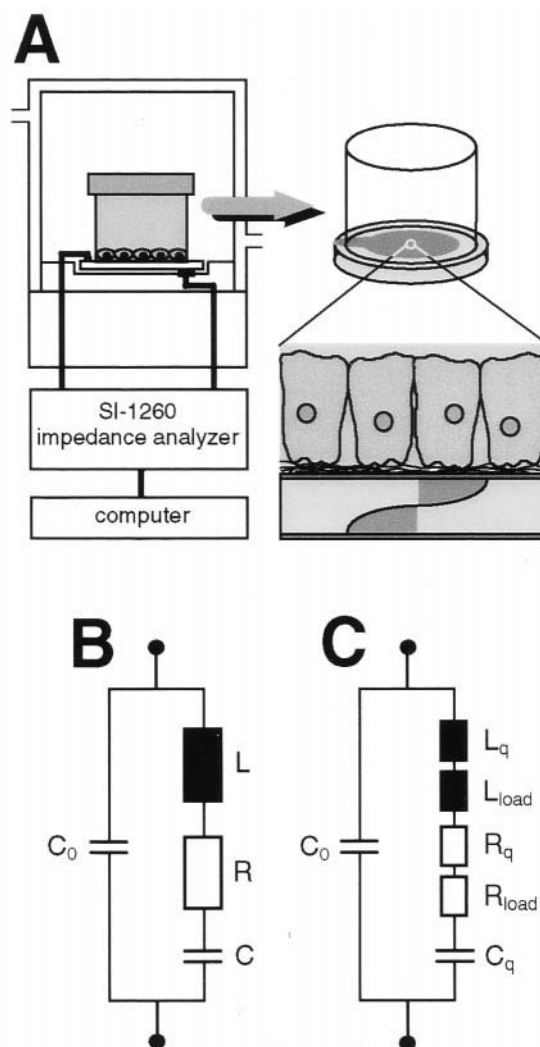

FIGURE 1 (*A*) Experimental setup to record impedance data of quartz resonators. As described previously (Janshoff et al., 1996), electrical contact with the gold electrode on the bottom side of the resonator was made with a copper ring that was integrated into the crystal holder. Contact with the gold electrode on the upper side of the resonator, which serves as a growth substrate, was achieved with a modified gold relay contact. (*B*) Butterworth-Van-Dyke (BVD) equivalent circuit. (*C*) Lumped-element equivalent circuit used to model the electrical characteristics of a quartz resonator in contact to a load material.

quartz material between the two surface electrodes, but it also contains parasitic contributions of the setup. The motional branch of the equivalent circuit dominates the total impedance of the resonator at frequencies close to resonance, whereas the parallel capacitance C_0 dominates the total impedance away from resonance. The transfer function of the BVD network was fitted to the recorded phase data $\phi(f)$ by nonlinear least-square methods (Levenberg-Marquardt algorithm). Only the capacitance C of the motional branch was fixed to a constant value of 21.655 fF during all fitting procedures, because it is exclusively determined by the material properties of quartz and the dimensions of the resonator (Noël and Topart, 1994; Janshoff et al., 1996b). The solid lines in Fig. 2 represent the transfer functions of the BVD equivalent circuit after parameter fitting.
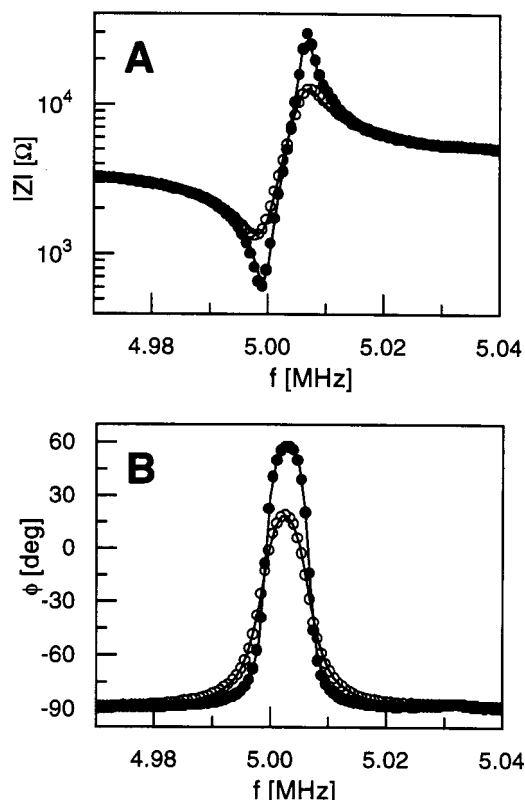
FIGURE 2   Bode presentation of impedance magnitude $|Z|$ (A) and phase shift ϕ (B) as a function of frequency for a 5-MHz quartz resonator near its fundamental resonance. Data for a resonator covered with a confluent layer of MDCK-II cells ($\bigcirc$) is compared with data for the same resonator after the cell layer has been removed ($\bullet$). For the sake of clarity not all of the 250 data points are plotted. Quantitative analysis yielded the following: $\bigcirc$, $R = 1603\ \Omega$, $L = 46.8128$ mH, $C_0 = 7.12$ pF; $\bullet$, $R = 650\ \Omega$, $L = 46.8056$ mH, $C_0 = 7.15$ pF. $T = 23°C$.

Cell culture

This study includes experiments with the epithelial cell line MDCK (strain I and II), primary cultured epithelial cells derived from porcine choroid plexus, the murine fibroblastic cell line 3T3 (Swiss), and bovine aortic endothelial cells (BAECs). The respective culture conditions are listed separately below. In all cases the medium of the stock cultures was exchanged twice a week. All subculturing of confluent cell layers used standard trypsinization (0.25% (w/v)) and centrifugation (110 × g) techniques. Before inoculation, the quartz dishes were treated with an argon plasma for 3–5 min, which provides both an intense cleaning of the gold surfaces and sterilization of the entire chamber.

MDCK-I and -II

We used Earle's minimum essential medium as the culture medium (Biochrom, Berlin, Germany) supplemented with 4 mM glutamine (Biochrom), 100 μg/ml each of penicillin and streptomycin (Biochrom), and 10% (v/v) fetal calf serum (Biochrom). Stocks of these cells were grown in incubators with a 5% CO_2 atmosphere.

Epithelial cells from porcine choroid plexus

Choroid plexus epithelial cells were isolated from the brains of freshly slaughtered pigs. Details of this preparation are given elsewhere (Gath et al., 1997). To improve the attachment, spreading, and growth of this cell type on the resonators, we coated the surface with 50 μg/ml laminin (Sigma, Deisenhofen, Germany) in water. Twenty-four hours after the cells were initially seeded, the cultures were washed with phosphate-buffered saline (1 mM Ca^{2+} and 0.5 mM Mg^{2+}) to remove erythrocytes. We used Dulbecco's minimum essential (DME)/HAM's F12 (1:1) basal medium (Bioconcept, Freiburg, Germany) supplemented with 10% (v/v) fetal calf serum, 4 mM L-glutamine, 5 μg/ml insulin (Sigma), 100 μg/ml each of penicillin and streptomycin, and 20 μM cytosine arabinoside (Sigma). The addition of cytosine arabinoside to the culture medium served to suppress contaminating fibroblasts (Gath et al., 1997). The cultures were kept in incubators with 5% CO_2 atmosphere.

3T3

Swiss 3T3 fibroblasts were grown in DMEM basal medium supplemented with 10% (v/v) fetal calf serum, 4 mM L-glutamine, and 100 μg/ml penicillin/streptomycin. These cells were kept in incubators with a 10% CO_2 atmosphere.

BAEC

Bovine aortic endothelial cells were obtained from Dr. S. Zink (Diabetes Forschungs-Institut, Düsseldorf, Germany). See Zink et al. (1993) for details of the isolation procedure. Cells were cultured in DMEM basal medium supplemented with 10% (v/v) fetal calf serum, 4 mM L-glutamine, and 100 μg/ml penicillin/streptomycin. Before inoculation quartz dishes and stock culture flasks were first flooded for at least 30 min with 0.5% (w/v) gelatin dissolved in phosphate-buffered saline (PBS) and then washed with PBS. Cells were grown in incubators with a 5% CO_2 atmosphere.

Adhesion assays

In one set of experiments we followed the attachment and spreading with time of initially suspended MDCK-II cells on the resonator surface with time. For this purpose confluent MDCK-II cell monolayers were washed twice with PBS (without divalent cations) and were then removed from the culture substrate by 0.25% (w/v) trypsin supplemented with 1 mM EDTA (10 min at 37°C). Trypsin digestion was terminated by the addition of an excess of complete culture medium. Cells were spun down at 290 × g for 10 min. The pellet was resuspended in culture medium, and aliquots of the cell suspension were transferred into the quartz dish after the cell number had been determined with a Bürker hemacytometer. When cell adhesion was studied in the presence of peptides related to one of the major integrin recognition sequences on extracellular matrix proteins Arg-Gly-Aps-Ser (RGDS), a corresponding amount of the peptide stock solution (in PBS; all purchased from Sigma) was added to the cell suspension inside the quartz dish. After the inoculated quartz was mounted in the crystal holder (37°C), impedance data were recorded continuously.

Removal of a cell layer but not the underlying extracellular matrix from a growth substrate

To probe the contribution of the extracellular matrix to the composite QCM response for an anchored cell monolayer, we used an experimental protocol that allowed us to remove the attached cells from their substrate, leaving their extracellular matrix behind (Kramer et al., 1985). The confluent cell layers were first incubated with deionized water for 30 min at room

temperature to gain hyposmotic cell lysis. The remaining cell debris was then removed by applying a phosphate buffer containing 1% (w/v) desoxycholate and 1% (w/v) Nonidet-P40 (Sigma) for 5–10 min. Light microscopic inspection of these substrates did not reveal any noticeable cell remains. Indirect immunostainings directed toward the extracellular matrix protein fibronectin, however, revealed the presence of this protein on the culture substrate in a network-like pattern (data not shown).

RESULTS

Preliminary remarks about QCM data analysis

It is one of the ultimate analytical goals of the QCM technique to extract mechanical properties of the material in contact with the resonator surface from measurements of the electrical characteristics of this piezoelectric device. The so-called Mason model (Rosenbaum, 1988) is currently regarded as the most accurate and versatile approach to such an analysis (Bandey et al., 1999), as it can be applied to composite multilayer systems. In this model the faces of the quartz resonator are represented as two acoustic ports that are connected by a transmission line representing phase shift and energy loss experienced by an acoustic wave during its propagation across the quartz thickness. The acoustic port on that side of the resonator that is covered with an overlayer material of any kind is terminated by a mechanical impedance $Z_{m,load}$. $Z_{m,load}$ is the ratio of shear stress imposed on the contacting material by the oscillating resonator to the resulting surface particle velocity (Bandey et al., 1999). $Z_{m,load}$ is therefore dependent on the mechanical characteristics of the material in contact with the resonator. The electromechanical coupling within the quartz plate is represented by a transformer that couples the acoustic ports of the resonator to an electrical port (surface electrodes), so that the mechanical properties of the resonator and the overlaying material can be inferred from electrical measurements. As long as the mechanical impedance of the surface load is small compared to the mechanical impedance of the quartz $Z_{m,q}$ ($Z_{m,load} \ll Z_{m,q}$), the distributed Mason model agrees closely with a much easier-to-handle equivalent circuit model with lumped impedance elements. This network describes the electrical properties of the unperturbed quartz resonator by the BVD-equivalent circuit and adds an additional impedance element Z_{load} into the motional branch to account for the surface loading. Z_{load} is proportional to its mechanical counterpart $Z_{m,load}$ according to

$$Z_{load} = \frac{\pi}{4 \cdot K^2 \cdot \omega_0 \cdot C_0} \cdot \frac{Z_{m,load}}{Z_{m,q}} \qquad (1)$$

with the electromechanical coupling constant K^2 and the angular resonance frequency ω_0. For the systems studied here it is difficult, if not impossible, to confirm the validity of the low load condition, but recent studies have shown that even for a heavy mass (≤ 5 mg/cm^2) or viscous loading ($\eta\rho \leq 1000$ g^2·cm^{-4}·s^{-1}), the lumped equivalent circuit is

still in very good agreement with the distributed Mason model (deviations $\leq 1\%$) (Bandey et al., 1997).

Both the mechanical impedance $Z_{m,load}$ and the electrical impedance Z_{load} are complex quantities. The real part of $Z_{m,load}$ corresponds to the component of surface stress in phase with surface particle velocity and therefore represents mechanical power dissipation at the surface. The imaginary part of $Z_{m,load}$ corresponds to the stress 90° out of phase with shear particle velocity and represents mechanical energy storage at the surface. The real and imaginary parts of the electrical impedance Z_{load} can be formally represented by a resistor R_{load} and an inductance L_{load} arranged in series, giving $Z_{load} = R_{load} + i \cdot \omega_0 \cdot L_{load}$. With

$$R_{load} = \frac{\pi}{4 \cdot K^2 \cdot \omega_0 \cdot C_0} \cdot \frac{Re(Z_{m,load})}{Z_{m,q}} \qquad (2)$$

and

$$L_{load} = \frac{\pi}{4 \cdot K^2 \cdot \omega_0^2 \cdot C_0} \cdot \frac{Im(Z_{m,load})}{Z_{m,q}} \qquad (3)$$

R_{load} is a direct measure of the dissipation of mechanical energy, whereas L_{load} is proportional to the mechanically stored energy at the resonator surface.

It is instructive to briefly consider two limiting cases of single-component loadings:

1. When the resonator surface is coated with a rigidly attached thin mass layer, the surface mechanical impedance is

$$Z_{m,load} = i \cdot \omega_0 \cdot m/A \qquad (4)$$

with the mass m deposited on a surface area A (Bandey et al., 1999). As the additional mass moves synchronously with the resonator surface, it increases the stored mechanical energy (kinetic energy) but does not lead to any energy dissipation ($Re(Z_{m,load}) = 0$). According to Eq. 3 the additional mass results in a proportional change of the inductance L_{load} and can be quantified from impedance measurements and parameter fitting.

2. When the resonator is loaded with a semiinfinite Newtonian fluid, the surface mechanical impedance is

$$Z_{m,load} = \sqrt{\omega_0 \cdot \rho_l \cdot \eta_l/2} \cdot (1 + i) \qquad (5)$$

with the liquid density ρ_l and its viscosity η_l (Bandey et al., 1999). As $Z_{m,load}$ contains real and imaginary components, the presence of a Newtonian fluid induces both energy dissipation and energy storage, which can be quantified from corresponding changes in R_{load} and L_{load}. The increased energy storage results from the movement of entrained liquid, whereas the power that is radiated into the viscously coupled liquid in the form of a damped shear wave causes energy dissipation.

Because it was our primary objective to identify the factors that contribute to the QCM response to attached cell

monolayers, we have empirically analyzed our data by using a lumped-element BVD-based equivalent circuit. Besides the impedance elements of the unperturbed resonator (C_0, R_q, C_q, L_q), the particular surface loading is accounted for by an additional resistance R_{load} and an additional inductance L_{load} within the motional branch of the circuit (Fig. 1 C). As it is impossible to directly extract the load-specific parameters R_{load} and L_{load} from a given impedance spectrum without further measurements, we either describe our experimental data in terms of the total resistance R ($R = R_q + R_{load}$) and the total inductance L ($L = L_q + L_{load}$) or in terms of changes of these two parameters (ΔR, ΔL) with respect to the values of the same resonator without cells but covered with culture medium. We chose this formalism, as a cell-free resonator covered with culture medium was usually the start or end point of any experiment providing a common basis without the necessity for further measurements. For the parallel capacitance C_0, determined by the dielectric properties of the quartz material and parasitic contributions due to wiring and crystal clamping, we have never observed any significant changes that could be attributed to the presence of cells on the quartz surface or any changes in their properties. This parameter is very sensitive, however, to any perturbations of the electrical contacts with the resonator and to the presence and position of an additional dipping electrode. As outlined above, the capacitance C ($C = C_q$) stays fixed during all data fitting. All other quantities that are commonly used in QCM studies (e.g., series and parallel resonance frequency, maximum admittance, dissipation factor) can be calculated from the numerical values for the four BVD parameters given here.

Analysis of different cell types at steady-state-like conditions

We first examined the individual impacts of different mammalian cell types on the characteristic parameters of the shear displacement. The cells were grown to confluence on top of the resonators, equilibrated to room temperature (23°C), and characterized by repeatedly recording impedance spectra. The cell layer was then thoroughly removed from the surface with a rubber policeman and a stream of medium. The cell-free, medium-loaded resonator was then measured again repeatedly. Table 1 summarizes the changes in resistance ΔR and inductance ΔL for the different cell types with respect to the medium-covered resonator. Changes in the motional resistance ΔR range from almost 1000 Ω for the epithelial MDCK-II cells to only 50 Ω for BAECs. For inductance changes ΔL, we observed a maximum average change of (16 ± 1.5) μH for epithelial cells derived from porcine choroid plexus and a minimum change of ~3 μH for both 3T3 fibroblasts and BAECs. It is apparent from the data in Table 1 that the presence of different cell species on top of the resonator induces significantly different and individual changes of shear wave pa-

TABLE 1 Changes in the motional resistance ΔR and the motional inductance ΔL that are associated with the presence of a confluent layer of the specified cell species with respect to the same resonator covered with cell culture medium only.

	ΔR (Ω)	ΔL (μH)	n
MDCK-I	755 ± 36	6.7 ± 0.7	8
MDCK-II	992 ± 36	10.5 ± 0.8	7
Choroid plexus	804 ± 43	16 ± 1.5	5
BAEC	55 ± 12	3.1 ± 0.5	5
3T3	277 ± 20	2.5 ± 0.5	5

A total of n different quartz resonators were examined for the respective cell type (±SDM). $T = 23$°C.

rameters. It was this observation that encouraged us to investigate the source of these differences in more detail, because a better understanding of the signal sources may disclose the entire potential of the QCM technique in cell biology.

Inhibition of specific, integrin-mediated adhesion to the resonator surface

We next addressed the question of whether anchorage and the subsequent spreading of the cells on the resonator surface are required to influence the shear displacement or if the sole presence of the cellular body in close proximity to the surface is already sufficient. To approach this question we added the pentapeptide Gly-Arg-Gly-Asp-Ser (GRGDS) in a 1 mM concentration to a suspension of MDCK-II cells (final seeding density 5×10^5 cm^{-2}) and followed the adhesion of these cells to the resonator surface by continuously recording impedance data. GRGDS is well known to competitively block the binding sites of several integrins (Pierschbacher and Ruoslahti, 1984), a group of transmembrane proteins known to anchor cells to certain extracellular matrix proteins. However, there was no need to precoat the resonator surfaces in these experiments as serum proteins from the culture medium, most notably vitronectin and fibronectin, adsorb to in vitro surfaces almost instantaneously (Vogler and Bussian, 1987). As a control for the specificity of the integrin blockade we performed the same experiment but added the pentapeptide Ser-Asp-Gly-Arg-Gly (SDGRG) in a 1 mM concentration to the seeding medium instead. SDGRG contains the same amino acids as GRGDS but in reverse order and therefore cannot interact specifically with the integrin-binding sites. Fig. 3 compares the time courses for the observed changes in motional resistance ΔR and inductance ΔL with respect to the initial parameters of the resonator loaded with culture medium only. In the presence of SDGRG (*empty circles*) the resistance (*A*) starts to increase ~20 min after cells were seeded and reaches a plateau value after 200 min. This time course was also obtained in the absence of peptides, indicating that SDGRG does not interfere with cell attachment behavior. Experiments using various microscopic techniques (phase
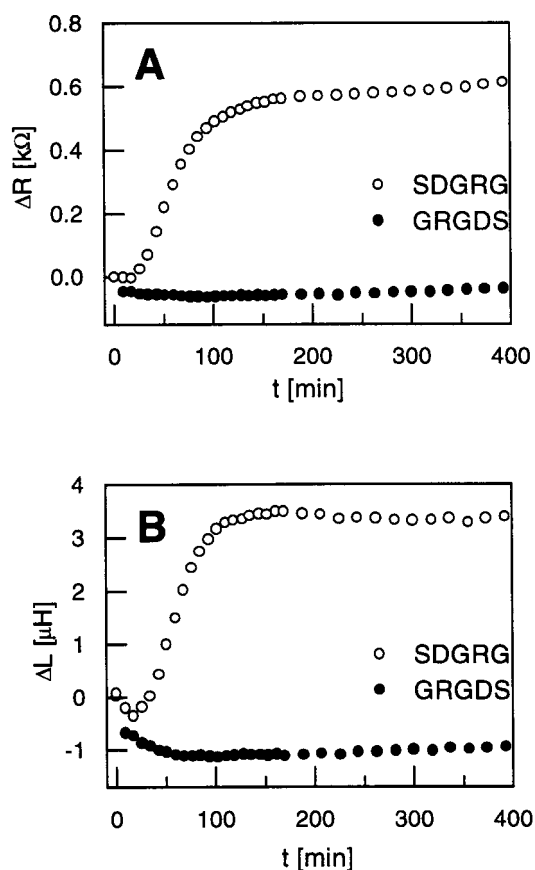
FIGURE 3 Change in resistance ΔR (*A*) and inductance ΔL (*B*) during the attachment of initially suspended MDCK-II cells in the presence of 1 mM GRGDS (●) or 1 mM SDGRG (○). The cells were seeded at a density of 5×10^5 cm^{-2} at time 0, and data acquisition was started immediately afterward. $T = 37°C$.

contrast, reflection interference contrast) confirmed that the increase in the motional resistance correlates strongly with the evolving surface coverage during attachment and spreading. The presence of 1 mM GRGDS (*filled circles*) completely abolishes any resistance increase, indicating that cells that are experimentally disabled to make integrin-mediated contacts with the protein-covered resonator surface have no measurable impact on the shear displacement. Microscopic inspection confirmed that these cells kept their spherical morphology and did not actively spread on the surface. The time courses of the inductance changes ΔL in Fig. 3 *B* show basically the same characteristics as described for the resistance before. The addition of GRGDS (*filled circles*) to the seeding medium effectively prevents an inductance increase like that seen with SDGRG (*empty circles*). The initial drop in both parameters at the beginning of each experiment arises from the warm-up of the culture medium in the temperature-controlled crystal holder and the coinciding decrease in the medium viscosity. We conclude that sedimentation of the cellular bodies to the resonator

surface and their loose interaction with the latter by non-specific interactions are not sufficient for detection by means of shear wave resonators. These findings are consistent with experiments published previously (Wegener et al., 1998) that used resonance frequency measurements.

Contribution of the extracellular matrix

As outlined in the preceding section, specific integrin-mediated adhesion is required for QCM detection of animal cells. Thus there has to be an immobilized layer of adhesion-promoting proteins between the cellular body and the resonator. These proteins can originate from a precoating of the resonator surface (as performed with choroid plexus epithelial cells and BAECs to support their adhesion), the spontaneous adsorption of serum proteins from the medium, or the secretion of extracellular proteins by the cells themselves.

We tried to quantify the contribution of this protein layer to the overall QCM response measured for cell-covered resonators. In a first approach we incubated the surface of a resonator for 24 h with a 50 μg/ml solution of collagen G in PBS to cover the substrate with a protein layer, as commonly used in tissue culture. The resonator was then equilibrated to room temperature and characterized by impedance data recordings. After removal of the protein layer with the same tools as for the cell layers before, the resonator was examined again. With respect to the resonator loaded with buffer only, the protein coating provides an additional resistance contribution of $\Delta R = (43 \pm 15)$ Ω and an inductance contribution of $\Delta L = (7.4 \pm 0.6)$ μH. Compared to the range of values obtained for entire cell layers, the resistance contribution is rather small, whereas the inductance contribution is considerable and well within the range that we observed for entire cell layers.

To quantify the contribution of the protein layer that actually exists beneath substrate-anchored cells, we applied an experimental protocol that allowed us to remove adherent cells from their culture substrate but to leave this protein cushion behind. It requires killing of the cells by hyposmotic lysis and removal of the remaining cell debris with a detergent-containing buffer (Kramer et al., 1985). In accompanying studies we experimentally verified by microscopic techniques (phase-contrast, indirect immunofluorescence) that the cell bodies were indeed removed by this experimental sequence, whereas fibronectin, for instance, could be clearly detected on the former culture substrate. Fig. 4, *A* and *B*, shows typical results for the changes in resistance and inductance derived from experiments with MDCK-I, MDCK-II, and 3T3 cells, in which we first characterized the resonator loaded with an intact cell layer (*filled columns*) and again after the cellular bodies were removed by the above-mentioned protocol (*open columns*). ΔR and ΔL denote the measured differences in the two parameters with respect to the same medium-loaded resonator after mechan-
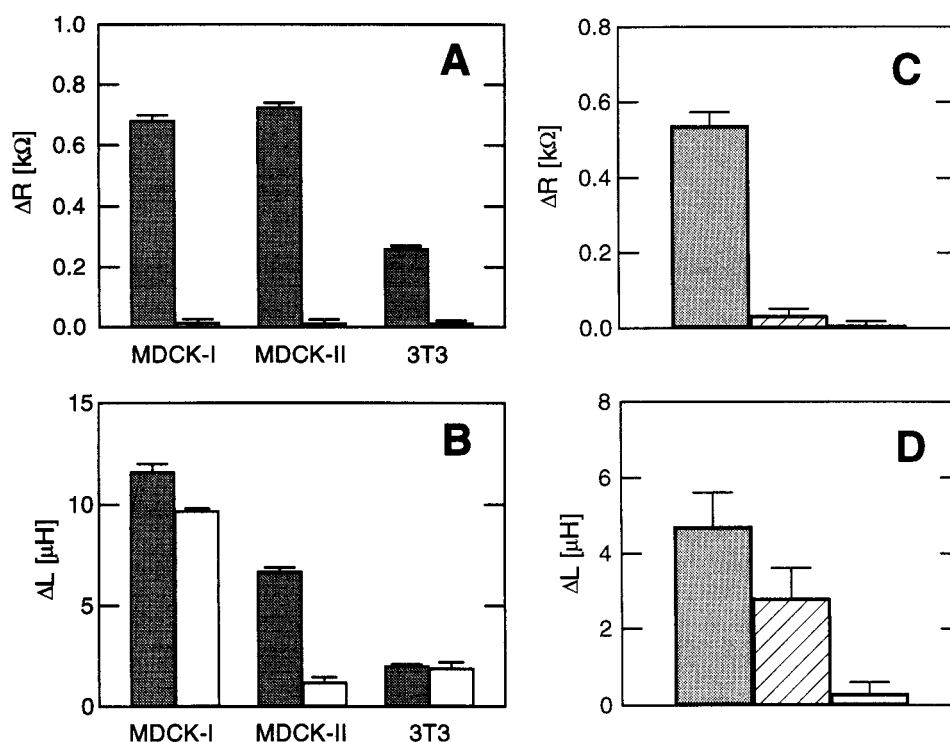
FIGURE 4 Typical resistance (*A*) and inductance (*B*) contribution of adhesion-promoting proteins beneath the cells. The filled columns represent the changes of the two parameters induced by a confluent cell layer of the specified type relative to the same resonator after mechanical cleaning and loading with medium only. The open columns show the remaining resistance and inductance contributions after the cell bodies were removed by hyposmotic cell lysis. The error bars correspond to the standard deviation of each parameter derived from repeated impedance data recordings. $T = 23°C$. *C* and *D* compare the corresponding shifts in resistance ΔR and inductance ΔL for a resonator covered with a confluent MDCK-II cell layer (*filled column*), after the cell bodies were removed by hyposmotic lysis (*hatched column*), and after an additional 10-min treatment of the surface with trypsin/EDTA (*open column*). Again, all shifts are given with respect to the same medium-loaded resonator after cleaning. $T = 23°C$.

ical cleaning. The presented data show consistently for all three cell types that removal of the cell bodies decreases the motional resistance to values that are less than 30 Ω above the level for the mechanically cleaned resonators. Looking at the inductances, however, reveals that removal of the cell bodies provides only a partial decrease in the measured values, which are well above readings for the medium-loaded resonators used as a reference. The remaining inductances can make up 90% of the inductance changes obtained for the entire cell layers (MDCK-I). Although we could observe this general phenomenon consistently, we noticed considerable variations in the partial inductance decrease after cell body removal, even among experiments with the same cell species.

To find further evidence that the remaining resistance and inductance contributions arise from extracellular matrix components, we treated the surface with trypsin after the cellular bodies were removed. Fig. 4, *C* and *D*, depicts the results of a typical experiment in which a confluent layer of MDCK-II cells was first removed from the quartz surface by hypotonic lysis. But before mechanical cleaning, the resonator surface was exposed to a 0.25% trypsin solution (including 1 mM EDTA) for 10 min and characterized by

impedance measurements afterward. The observed changes in resistance ΔR and inductance ΔL (both with respect to the mechanically cleaned, medium-loaded resonator) support the idea that the remaining inductance contributions after removal of the cellular bodies are of proteinaceous origin, as they completely disappear upon trypsin digestion.

Contributions of the actin cytoskeleton

A network of filamentous actin underlies the plasma membranes of mammalian cells (cell cortex) and is regarded to be of crucial importance for their mechanical properties (Bray, 1992), which themselves are very likely to contribute to the QCM response. Besides this membrane-bound network, actin also arranges in the form of thick bundles, the so-called stress fibers, which interconnect different sites of focal adhesion to the substrate. We investigated the possibility that disruption of the actin cytoskeleton via the fungal toxin cytochalasin D alters the QCM parameters of attached cells. In Fig. 5 motional resistance *R* and inductance *L* are traced versus time for a typical experiment in which a confluent layer of MDCK-II cells was treated with 5 μM
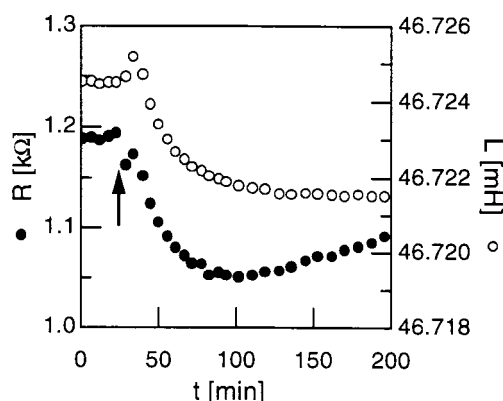
FIGURE 5   Time course of the resistance R (●) and the inductance L (○) when a confluent monolayer of MDCK-II cells is treated with 5 μM cytochalasin D (*arrow*). $T = 37°C$.

cytochalasin D (*arrow*). The resistance R drops from a baseline value of ~1200 Ω to a transient minimum of 1050 Ω within 75 min and starts to recover afterward. The inductance drops with a somewhat slower kinetic by 3 μH but apparently does not show any recovery. Control experiments in which the cell layers were treated with a corresponding amount of pure dimethyl sulfoxide that was used as a solvent for cytochalasin D did not show these changes in R and L. Only the initial spike-like changes of both parameters immediately after cytochalasin D addition (short increase in inductance, decrease in resistance) were observable. To correlate these time courses with the actual disruption of the actin cytoskeleton, we performed microscopic studies using the fluorescently labeled actin marker tetramethylrhodamine isothiocyanate-phalloidin. Fig. 6 shows

fluorescence micrographs of MDCK-II cells that were exposed to 5 μM cytochalasin D for 0 (Fig. 6 *A*), 25 (Fig. 6 *B*), 75 (Fig. 6 *C*), and 100 min (Fig. 6 *D*) before fixation and phalloidin staining. Images were taken with a confocal laser scanning microscope, and the focal plane was adjusted to the basal cell membrane. In Fig. 6 *A* the actin bundles inside the unchallenged cells can clearly be seen to run almost parallel to the substrate plane, and the actin cortex is visible as a ring along the cell perimeter. After 25 min of cytochalasin D exposure, the majority of the stress fibers have been degraded to point-like structures, but some fibers are still visible. A 75-min exposure to the drug results in an almost complete absence of the fibers, and this situation is unchanged for the 100-min sample. Comparison between these microscopic images and the time course of the QCM parameters strongly supports the idea that the QCM technique is capable of probing changes in the actin cytoskeleton close to the basal cell membrane.

Medium overlaying the cells

To describe the composite cell resonator system in terms of a mechanical model, it is important to know whether the medium that overlays the cell layer contributes to the QCM response. Thus we changed the mechanical properties of the overlaying medium and monitored the response of the QCM. It is important to guarantee in this experiment that medium modifications do not interfere with the normal morphology of the anchored cells. We therefore added polyvinylpyrrolidone (PVP) (molecular mass = 360 kDa) in a final concentration of 1% (w/v) to the culture medium, which increases its viscosity considerably without significant changes to its osmolarity. PVP is known, furthermore,

FIGURE 6   Fluorescence micrographs of confluent MDCK-II cell layers in which the actin cytoskeleton was stained with fluorescently labeled phalloidin to visualize its changes during exposure to cytochalasin D. Micrograph *A* shows cells that were not exposed to cytochalasin D at all. Exposure to 5 μM cytochalasin D for (*B*) 25 min, (*C*) 75 min, and (*D*) 100 min results in the depicted alterations of the actin network. The scale bar corresponds to 25 μm. $T = 37°C$.
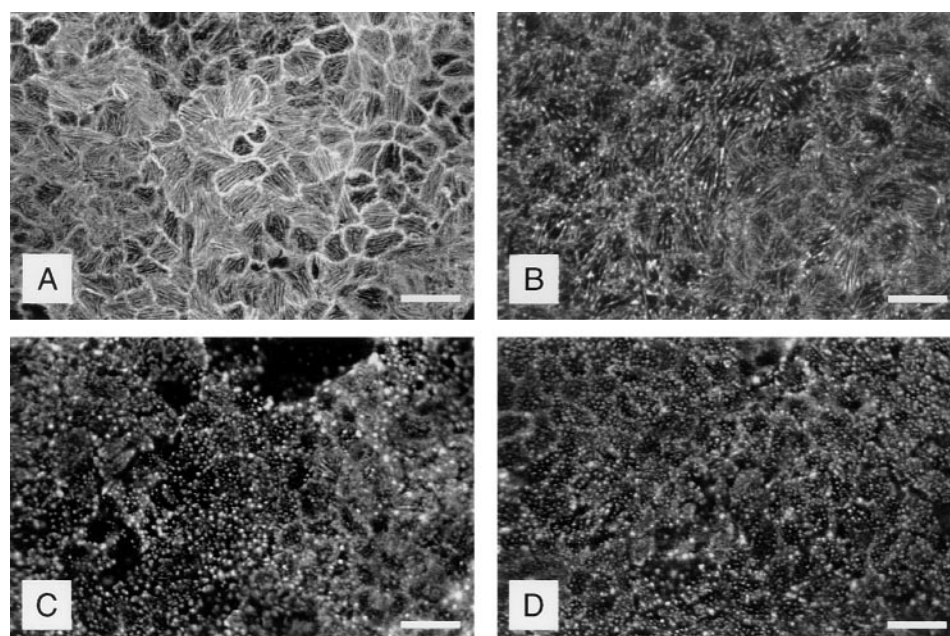
for its cell compatibility. To quantify the associated viscosity change due to PVP addition, we used the QCM as a viscometer and calibrated our setup (compare Eq. 5) by measuring the motional resistance R as a function of the known density-viscosity products of different glycerol/water mixtures (Janshoff et al., 1996b). The viscosity of a fluid of interest is then accessible from readings for the motional resistance and an independent determination of its density (Gay-Lussac pyknometer). After replacing ordinary culture medium in contact with a quartz resonator by culture medium containing 1% PVP, the motional resistance increased by (383 ± 12) Ω, which is equivalent to a change in viscosity from 0.011 g/cm·s for medium without PVP to an apparent viscosity of 0.042 g/cm·s for medium with PVP (We prefer to use the term "apparent viscosity" for PVP-containing solutions, as we did not consider frequency-dependent viscous effects due to PVP addition.) In the same type of replacement experiment with a quartz resonator covered with a confluent layer of MDCK-II cells, the motional resistance increased by only (26 ± 13) Ω, while the inductance decreased by (0.6 ± 0.6) μH. As the changes in both parameters are barely significant when the apparent viscosity of the medium on top of the cell layer is changed by a factor of 4, we conclude that the overlaying medium does not contribute to the overall QCM response to MDCK-II cells and that the shear wave does not escape the cellular bodies with significant amplitude.

We also determined the height of all cell species that were used in this study by confocal laser scanning microscopy. MDCK-II cells, which were used in PVP experiments, were found to have the smallest average height $((4.5 \pm 1)$ $\mu m)$ of all cell types examined (BAECs are excluded from this comparison, as these cells behave differently for reasons discussed later). As the shear wave does not propagate across MDCK-II cells, although they show the highest impact on the motional resistance (Table 1) and the least height, we conclude that this is also true for all other cell types in this study with lower motional resistances and increased cell heights.

Application of hyperosmotic media

Data presented thus far clearly demonstrate that cell layers dissipate motional energy from the resonator and therefore behave like a lossy and viscous material. More recent studies by Periasamy et al. (1992) have shown that the cytoplasmic viscosity of adherent MDCK cells increased by 50% when the cells were kept in hyperosmotic culture medium (1200 mOsm/kg H_2O). We therefore examined the changes in QCM parameters when confluent cell layers were challenged with hyperosmotic media. Fig. 7 shows the time courses of the motional resistance and inductance for a confluent layer of MDCK-I cells when the osmolarity of the culture medium was gradually increased from 290 (isotonic) to 415 (1), to 560 (2), and to 1100 mOsm/kg H_2O (3) and
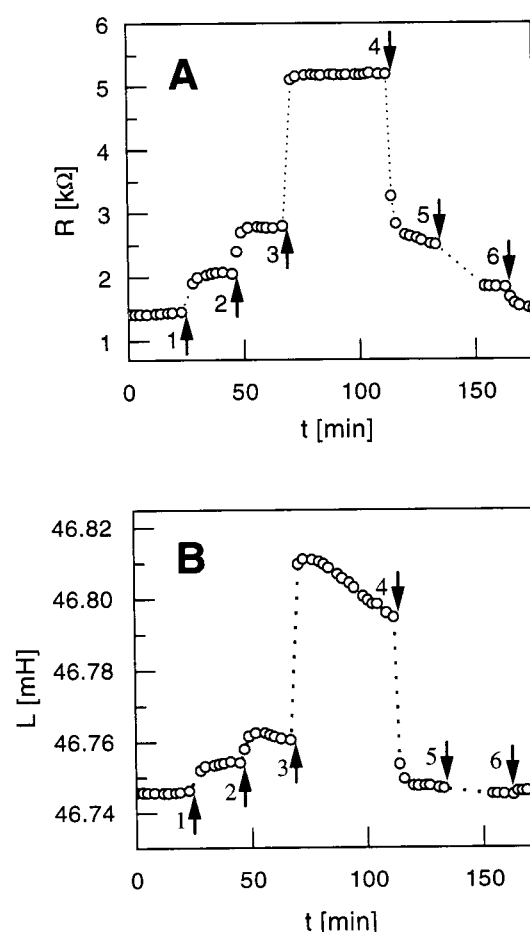

FIGURE 7 Time course of motional resistance R (A) and inductance L (B) when the osmolarity of the culture medium covering a confluent monolayer of MDCK-I cells is gradually increased from 290 mOsm/kg H_2O (isotonic) to 415 mOsm/kg H_2O (1), to 560 mOsm/kg H_2O (2), to 1100 mOsm/kg H_2O (3) and subsequently back to isotonic conditions in the same steps (4–6). $T = 23°C$.

subsequently decreased through a reversal of the same steps (4–6). The osmolarity of the medium was adjusted by adding corresponding amounts of sucrose and verified by freezing point depression. Control experiments in which we performed exchanges from isotonic back to isotonic medium (not shown) ensured that the exchange procedure itself did not provide measurable disturbances. An increase in medium osmolarity leads to dose-dependent, reversible, and very pronounced increases in both the motional resistance and the motional inductance. Note that the motional resistance increases in an almost step-like manner and has increased by 3500 Ω when medium with the highest osmolarity is applied. For comparison, the motional resistance of a cell-free resonator changes by only ~150 Ω under the same experimental conditions. The observed changes in resistance were highly reproducible, whereas we have found minor but noticeable deviations in the inductance changes—especially within the exact time profiles—when repetition

experiments were performed. We extended these studies to confluent MDCK-II and 3T3 cell layers and focused on the more reproducible alterations of the motional resistance. Fig. 8 compares the relative resistance changes measured for the two epithelial cell species with those obtained for fibroblastic 3T3 cells, when the medium osmolarity was altered from isotonic to the specified hyperosmotic value. For all three cell species the motional resistance increases linearly with medium osmolarity. Although quite different in cell dimensions and morphology, MDCK-II cells behave very similarly compared with MDCK-I cells in these experiments, and we observed a ~3.5-fold increase in motional resistance for the highest osmolarity applied. The fibroblastic 3T3 cells, however, responded distinctly differently, and the motional resistance increased by less than twofold for the highest osmolarity. Preliminary measurements of the associated cell volume changes for these three cell types have not shown significant differences in the degree of cell shrinkage or osmotolerance. We therefore suggest that the restricted diffusion of hydrophilic compounds across epithelial cell layers due to the formation of tight intercellular junctions is mainly responsible for the observed differences. In the following Discussion section we will introduce our understanding of these particular data, based on the insights we gained from all experiments mentioned in this paper.

DISCUSSION

In one of the first reports on using the QCM technique to probe anchorage of mammalian cells to an artificial substrate, Redepenning et al. (1993) demonstrated that the attachment and spreading of cells on a resonator surface gave rise to considerable changes of the resonance frequency ($\Delta f \approx 500$ Hz with $f_0 = 5$ MHz). These frequency shifts were, however, significantly smaller than expected from the Sauerbrey equation for the actual cell mass ($\sim$ 10000 Hz):

$$\Delta f = \frac{-2 \cdot f_0^2 \cdot \Delta m}{A \cdot \sqrt{\mu_q \cdot \rho_q}} \qquad (6)$$

with electrode surface area A, shear stiffness of quartz μ_q, and its density ρ_q. Because the Sauerbrey equation is only valid when a thin layer of a foreign material is homogeneously and rigidly deposited on the device surface (e.g., an evaporated metal film), the observed discrepancy was the first hint that cells might not simply behave like an additional mass layer. In an initial impedance study (Janshoff et al., 1996b) we were able to show that the presence of a confluent cell layer attached to the resonator increased both energy dissipation (ΔR) and energy storage (ΔL) at the crystal surface. This observation indicated that the cell layer has to be treated like a lossy overlayer material rather than a rigid mass, which would only alter the motional inductance (compare Eq. 4). Our findings were later independently confirmed by Fredriksson et al. (1998), who used simultaneous resonance frequency and dissipation factor measurements. We tried to interpret the observed changes of R and L mechanically by treating the cell layer as a semi-infinite layer of an entirely viscous material with a wetting-like contact with the resonator surface (Janshoff et al., 1996b). However, the applied model assumption could not explain all experimental observations, as we found inconsistencies between the observed changes in R and L and those predicted by the model. We concluded that the development of a more detailed and appropriate model for such a complex system like an attached cell monolayer requires first of all an understanding of what parts of the cellular body and its adhesion machinery contribute to the overall QCM response. This knowledge should also disclose possible applications and limitations of this technique in fundamental cell biology as well as biotechnology.

The data summarized in Table 1 provide a strong first indication of the importance of cell-substrate interactions for QCM measurements with mammalian cells. The highest impact on the load resistance R was found for epithelial cell layers (MDCK-I, MDCK-II, choroid plexus epithelial cells), whereas 3T3 fibroblasts cause significantly lower resistance changes, and BAECs are barely detectable. From handling and observing BAECs in routine cell culture, we already noticed that these cells were only weakly anchored to the surface and were easily detached form their culture substrate as intact sheets. This indicates that intercellular contacts between BAECs were more resistant to mechanical stress than were their interactions with the substrate. As reported earlier (Wegener et al., 1999), we also learned from cross-sectional images using confocal laser scanning microscopy that these cells show a very large spacing of more
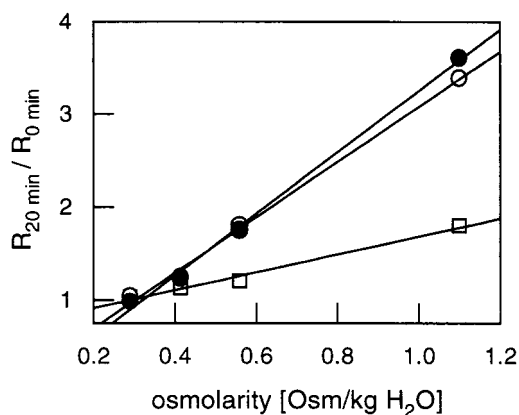

FIGURE 8   Increase in the motional resistance as a function of medium osmolarity for MDCK-I (○), MDCK-II (●), and 3T3 cell layers (□). The resistance value measured 20 min (R_{20min}) after isotonic medium was exchanged for medium of specified osmolarity normalized to its value immediately before medium exchange (R_{0min}). Each data point represents the average result of two experiments. $T = 23°C$.

than 500 nm between their basal plasma membrane and the substrate. Keeping in mind that the shear wave that is launched from the resonator surface into pure culture medium of density ρ_{med} and viscosity η_{med} has a characteristic decay length $\delta = \{2 \cdot \eta_{\mathrm{med}}/(\omega \cdot \rho_{\mathrm{med}})\}^{1/2}$ of ~ 250 nm, these cell layers are obviously too far from the substrate to be reached by the shear wave with considerable amplitude. Epithelial cells, however, tend to attach very firmly to artificial surfaces with small average cell-substrate separation distances (Lo et al., 1995). Fibroblasts show only small areas of close adhesion to the substrate (<30 nm), whereas the remaining areas of the basal plasma membrane are farther apart (Parak et al., 1999). The resistance data in Table 1 can be arranged in a similar order, supporting the concept that cell-substrate separation distance and actual contact area are decisive for the outcome of QCM experiments.

The adhesion experiments in the presence of the GRGDS pentapeptide that blocks integrin-binding sites and prevents the cells from forming close contacts with the resonator surface are entirely consistent with this viewpoint. Assuming a homogeneous distribution of the spherical cells on the resonator surface and their radius r_{c} to be 5.8 μm (Wegener et al., 1998), the seeding density applied in the experiment (Fig. 3) was formally sufficient to cover $\sim 70\%$ of the available surface area, but the shear displacement was apparently not affected. Because of the spherical morphology of the cells under these conditions, only a small portion of the basal plasma membrane is at the smallest distance from the surface, and the separation distance itself may be considerably enlarged as specific interactions are omitted. It is interesting to correlate these results with combined QCM/scanning force microscopy (SFM) studies that were directed toward vesicle adsorption (Pignataro et al., 2000). It was found that the frequency shift associated with the adsorption of receptor doped vesicles (large unilamellar vesicles) on a resonator surface made functional with immobilized ligands increased with the amount of receptors incorporated into the liposome shells. SFM studies on the same model system revealed a concomitant increase of the contact area between the adsorbed vesicles and the substrate, which is therefore responsible for the observed QCM response.

The development of an appropriate electromechanical model for animal cells cultured on acoustic devices requires identification of the respective signal contributions of all major components in this composite system. Therefore our findings that the protein film between a basal cell membrane and a surface may have considerable influence on the response of shear mode resonators are crucial for further interpretation of QCM data in terms of viscoelastic properties of the attached cells. It has been shown repeatedly for various model systems that the QCM is sensitive enough to detect the specific adsorption of small amounts of protein to the resonator surface, for instance, binding of antibodies to immobilized antigens (Rickert et al., 1997; Muramatsu et al., 1987) or binding of bacterial toxins to their immobilized

receptors (Janshoff et al., 1997). These previous studies underline the necessity to consider preadsorbed or secreted protein beneath the cells and are in complete agreement with the data presented here.

We have found consistently, for either preadsorbed collagen films or the extracellular matrix underneath the cells, that the presence of adsorbed proteins induces significant changes in the motional inductance and minor changes in the motional resistance compared to the values for intact cell layers. However, according to Eq. 4 an ideal mass load of the resonator causes changes only in the motional inductance. The small but measurable effects of the protein films on the motional resistance may be due to 1) trapped liquid that moves inside or in and out of the porous protein assembly or 2) the viscoelastic properties of the protein itself (Rodahl et al., 1997). Because of these deviations from ideal mass behavior, the impedance contributions of the extracellular matrix and those of the complete cell layers cannot be treated in a strictly linear fashion (Bandey et al., 1999), as a dissipative layer close to the resonator surface causes an acoustic phase shift that affects the impedance contributions of all upper layers. The observed variations in rest inductance after the cell bodies were experimentally removed will be addressed in future studies. It is important to understand whether these variations are indeed caused by different amounts of protein beneath the cells, whether the experimental sequence applied here does not consistently leave all of the extracellular protein behind, or whether an even more involved explanation applies.

Anchorage of mammalian cells to protein-coated artificial substrates is mainly accomplished by integrins. These transmembrane proteins are intracellularly connected to the actin cytoskeleton that underlies the plasma membrane. It is this connection to the actin network that delocalizes and distributes mechanical forces over the entire cell body and thereby provides the mechanical stability of cell-substrate contacts (Bray, 1992). The fluorescent micrographs in Fig. 6 show the well-known effect by cytochalasin D of disrupting the actin cytoskeleton inside the cell and reducing former fibers to point-like actin accumulations. Comparison between the stage of actin disrupture and the impact on shear wave parameters (Fig. 5) at corresponding times strongly indicates that the actin depolymerization can be detected by the QCM technique. It remains, however, an open question whether the associated alterations of the mechanical stiffness of the plasma membrane or induced changes in the adhesion pattern are ultimately responsible for this phenomenon.

The cell-type-specific QCM response, when confluent cell layers were exposed to hyperosmotic media, is another important result of this study. As is apparent from Fig. 8, these experiments revealed significant differences between the epithelial MDCK cells (both strains) and the fibroblastic 3T3 cells. We have already mentioned above that different sensitivities to hyperosmotic conditions in terms of a dif-

ferent degree of cell shrinkage are unlikely sources for these observations. However, in contrast to fibroblastic 3T3 cells, the epithelial MDCK cells express tight intercellular junctions. These so-called tight junctions (Wegener and Galla, 1996) occlude the intercellular diffusion pathway and thereby enable epithelial cell layers to act as a selective barrier between two different fluid compartments. Accordingly, the permeation rate of a membrane-impermeable probe across the cell layer is lowered considerably for barrier-forming cell types. For MDCK-I and MDCK-II cells we found that the permeation rate of radiolabeled sucrose amounts to $(1.5 \pm 0.1) \times 10^{-7}$ cm/s and $(0.9 \pm 0.2) \times 10^{-7}$ cm/s, respectively, whereas the corresponding value for 3T3 cells is roughly two orders of magnitude larger and amounts to $(1.6 \pm 0.3) \times 10^{-5}$ cm/s. Thus, in the case of barrier-forming MDCK cells (both strains), the diffusion of sucrose, which was used to increase medium osmolarity, along the intercellular cleft is limited, and the osmotic pressure drags the water not only out of the cellular bodies but also out of the water-filled compartments beneath the cells (Fig. 9). This phenomenon of osmotically induced transepithelial water transport is well known for a variety of epithelia (Reuss, 1991). Water loss in the channel between cell and substrate may then result in a decrease in the average cell-substrate separation distance, and the remaining water may become highly immobilized. Both processes are likely to produce alterations in the QCM parameters as they were actually observed (Fig. 7). In agreement with the data presented in Fig. 8, the proposed mechanism does not apply to the same degree to fibroblastic cells with open intercellular clefts. We conclude that the mechanical properties and the dimensions of the liquid- and protein-filled channels between cell and substrate have to be taken into account when QCM data of anchorage-dependent cells are discussed. It is interesting to note in this context that the viscosity within this aqueous compartment beneath attached cells has been estimated to range between 0.01 and 1 g/cm·s (Gallez, 1994) and can therefore exceed the bulk viscosity of water considerably.

The development of an appropriate model for analyzing QCM data of animal cells more comprehensively is ongoing. Based on our current understanding, we think that such a model has to include at least three nonpiezoelectric layers: 1) the water-and-protein-filled compartment beneath the cells, 2) the cell membrane itself, and 3) the underlying actin cytoskeleton. The rather complex mechanical interactions between these layers provide additional complications.

CONCLUSION

The response of shear wave resonators to mammalian cell adhesion is dependent on a specific, receptor-mediated interaction of the cells with extracellular matrix proteins adsorbed or secreted to the quartz surface. Our studies revealed that extracellular matrix deposition (or precoating), the integrity of the actin cytoskeleton, cell-substrate separation distance, and, presumably, the mechanical properties of the narrow cleft between cell and substrate have their individual impacts on the composite result of QCM measurements. However, changes in the mechanical properties of the fluid that contacts the apical cell surface do not influence QCM parameters. We conclude that the QCM approach is only capable of probing those parts of the cellular body that are involved in cell-substrate interactions. For studies directed toward this particular aspect of living cells in culture, the QCM technique provides an integral, quantitative, and noninvasive tool. As the morphology of animal cells—probably one of the most sensitive indicators for their health and metabolic state—is directly related to the degree and strength of cell-substrate interactions, the QCM technique may also be used as a transducer in drug development and toxicity assays.
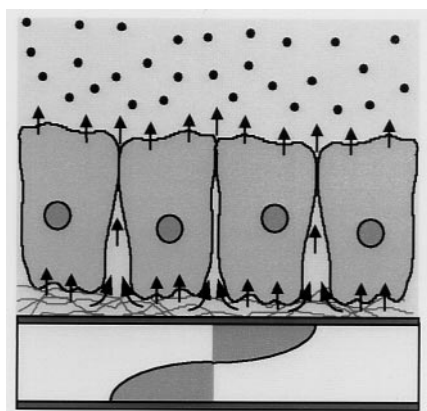

FIGURE 9 Osmotically induced water withdrawal from the fluid compartment between barrier-forming cells and their growth substrate. Water loss may decrease the separation distance between basal cell membrane and substrate and enhance immobilization of the remaining water in this narrow, protein-filled channel. The arrows indicate the direction of water flow.

REFERENCES

Bandey, H. L., A. R. Hillman, M. J. Brown, and S. J. Martin. 1997. Viscoelastic characterization of electroactive polymer films at the electrode/electrolyte interface. *Faraday Discuss.* 107:105–121.

Bandey, H. L., S. J. Martin, R. W. Cernosek, and A. R. Hillman. 1999. Modeling the responses of thickness-shear mode resonators under various loading conditions. *Anal. Chem.* 71:2205–2214.

Bray, D. 1992. Cell Movements. Garland Publishing, New York and London.

Buttry, D. A., and M. D. Ward. 1992. Measurement of interfacial processes at electrode surfaces with the electrochemical quartz crystal microbalance. *Chem. Rev.* 92:1355–1379.

Fredriksson, C., S. Kihlman, M. Rodahl, and B. Kasemo. 1998. The piezoelectric quartz crystal mass and dissipation sensor: a means of studying cell adhesion. *Langmuir.* 14:248–251.

Gallez, D. 1994. Non-linear stability analysis for animal cell adhesion to solid supports. *Colloids Surf. B Biointerfaces.* 2:273–280.

Gath, U., A. Hakvoort, J. Wegener, S. Decker, and H.-J. Galla. 1997. Porcine choroid plexus cells in culture: expression of polarized phenotype, maintenance of barrier properties and apical secretion of CSF-components. *Eur. J. Cell Biol.* 74:68–78.

Gryte, D. M., M. D. Ward, and W.-S. Hu. 1993. Real-time measurement of anchorage dependent cell adhesion using a quartz crystal microbalance. *Biotechnol. Prog.* 9:105–108.

Janshoff, A., C. Steinem, M. Sieber, A. el Bayâ, M. A. Schmidt, and H.-J. Galla. 1997. Quartz crystal microbalance investigation of the interaction of bacterial toxins with ganglioside containing solid supported membranes. *Eur. Biophys. J.* 26:261–270.

Janshoff, A., C. Steinem, M. Sieber, and H.-J. Galla. 1996a. Specific binding of peanut agglutinin to G_{M1}-doped solid supported lipid bilayers investigated by shear wave resonator measurements. *Eur. Biophys. J.* 25:105–113.

Janshoff, A., J. Wegener, M. Sieber, and H.-J. Galla. 1996b. Double-mode impedance analysis of epithelial cell monolayers cultured on shear wave resonators. *Eur. Biophys. J.* 25:93–103.

Kramer, R. H., G. M. Fuh, K. G. Bensch, and M. A. Karasek. 1985. Synthesis of extracellular matrix glycoproteins by cultured endothelial cells isolated from the dermis of neonatal and adult skin. *J. Cell Physiol.* 123:1–9.

Lo, C.-M., C. R. Keese, and I. Giaever. 1995. Impedance analysis of MDCK cells measured by electric cell-substrate impedance sensing. *Biophys. J.* 69:2800–2807.

Martin, S. J., V. E. Granstaff, and G. C. Frye. 1991. Characterization of a quartz crystal microbalance with simultaneous mass and liquid loading. *Anal. Chem.* 63:2272–2281.

Muramatsu, H., J. M. Dicks, E. Tamiya, and I. Karube. 1987. Piezoelectric crystal biosensor modified with protein A for determination of immunoglobulins. *Anal. Chem.* 59:2760–2763.

Noël, A. M., and P. A. Topart. 1994. High frequency impedance analysis of quartz crystal microbalances. I. General considerations. *Anal. Chem.* 66:484–491.

Parak, W. J., J. Domke, M. George, A. Kardinal, M. Radmacher, H. E. Gaub, A. D. G. de Roos, A. P. R. Theuvenet, G. Wiegand, E. Sackmann, and J. C. Behrends. 1999. Electrically excitable normal rat kidney fibroblasts: a new model system for cell-semiconductor hybrids. *Biophys. J.* 76:1659–1667.

Periasamy, N., H. Pin Khao, K. Fushimi, and A. S. Verkman. 1992. Organic osmolytes increase cytoplasmic viscosity in kidney cells. *Am. J. Physiol.* 263:C901–C907.

Pierschbacher, M. D., and E. Ruoslahti. 1984. Cell attachment activity of fibronectin can be duplicated by small synthetic fragments of the molecule. *Nature.* 309:30–33.

Pignataro, B., C. Steinem, H.-J. Galla, H. Fuchs, and A. Janshoff. 2000. Specific adhesion of vesicles monitored by scanning force microscopy and quartz crystal microbalance. *Biophys. J.* 78:474–486.

Redepenning, J., T. K. Schlesinger, E. J. Mechalke, D. A. Puleo, and R. Bizios. 1993. Osteoblast attachment monitored with a quartz crystal microbalance. *Anal. Chem.* 65:3378–3381.

Reuss, L. 1991. Tight junction permeability to ions and water. *In* Tight Junctions. M. Cereijido, editor. CRC Press, Ann Arbor, MI.

Rickert, J., A. Brecht, and W. Göpel. 1997. Quartz crystal microbalances for quantitative biosensing and characterization of protein multilayers. *Biosens. Bioelectron.* 12:567–575.

Rodahl, M., F. Höök, C. Fredriksson, C. A. Keller, A. Krozer, P. Brzezinski, M. Voinova, and B. Kasemo. 1997. Simultaneous frequency and dissipation factor QCM measurements of biomolecular adsorption and cell adhesion. *Faraday Discuss.* 107:229–246.

Rosenbaum, J. F. 1988. Acoustic Wave Theory and Devices. Artech House, Boston.

Sauerbrey, G. 1959. Verwendung von Schwingquarzen zur Wägung dünner Schichten und zur Mikrowägung. *Z. Phys.* 155:206–222.

Vogler, E. A., and R. W. Bussian. 1987. Short-term cell attachment rates: a surface sensitive test of cell-substrate compatibility. *J. Biomed. Mater. Res.* 21:1197–1211.

Wegener, J., and H.-J. Galla. 1996. The role of non-lamellar lipid structures in the formation of tight junctions. *Chem. Phys. Lipids.* 81:229–255.

Wegener, J., A. Janshoff, and H.-J. Galla. 1998. Cell adhesion monitoring using a quartz crystal microbalance: comparative analysis of different mammalian cell lines. *Eur. Biophys. J.* 28:26–37.

Wegener, J., S. Zink, P. Rösen, and H.-J. Galla. 1999. Use of electrochemical impedance measurements to monitor β-adrenergic stimulation of bovine aortic endothelial cells. *Pflügers Arch. Eur. J. Physiol.* 437:925–934.

Yang, M., and M. Thompson. 1993. Multiple chemical information from the thickness shear mode acoustic wave sensor in the liquid phase. *Anal. Chem.* 65:1158–1168.

Zink, S., P. Rösen, B. Sackmann, and H. Lemoine. 1993. Regulation of endothelial permeability by β-adrenoceptor agonists: contribution of β_1- and β_2-adrenoceptors. *Biochim. Biophys. Acta.* 1178:286–298.